DLDTI: A Learning-based Framework for Drug-target Interaction Identification Using Neural Networks and Network Representation

Yihan Zhao
Department of Graduate School, Beijing University of Chinese Medicine, Beijing, China
Kai Zheng
School of Computer Science and Engineering, Central South University, Changsha, China
Baoyi Guan
National Clinical Research Center for Chinese Medicine Cardiology, Xiyuan Hospital, China Academy of Chinese Medical Sciences, Beijing, China
Mengmeng Guo
Institute of Cardiovascular Sciences, Health Science Center, Peking University, Key laboratory of Molecular Cardiovascular Sciences, Ministry of Education, Beijing, China
Lei Song
Department of Graduate School, Beijing University of Chinese Medicine, Beijing, China
Jie Gao
National Clinical Research Center for Chinese Medicine Cardiology, Xiyuan Hospital, China Academy of Chinese Medical Sciences, Beijing, China
Hua Qu
National Clinical Research Center for Chinese Medicine Cardiology, Xiyuan Hospital, China Academy of Chinese Medical Sciences, Beijing, China
Yuhui Wang
Institute of Cardiovascular Sciences, Health Science Center, Peking University, Key laboratory of Molecular Cardiovascular Sciences, Ministry of Education, Beijing, China
Dazhuo Shi
National Clinical Research Center for Chinese Medicine Cardiology, Xiyuan Hospital, China Academy of Chinese Medical Sciences, Beijing, China
Ying Zhang (echo993272@sina.com)
China Academy of Chinese Medical Sciences https://orcid.org/0000-0002-7549-3968

Research

Keywords: drug-target interaction, heterogeneous information, network representation learning, stacked auto-encoder, deep convolutional neural networks, atherosclerosis

Posted Date: August 19th, 2020

DOI: https://doi.org/10.21203/rs.3.rs-56700/v1

Version of Record: A version of this preprint was published on November 13th, 2020. See the published version at https://doi.org/10.1186/s12967-020-02602-7.

DLDTI: A learning-based framework for drug-target interaction identification using neural networks and network representation

Yihan Zhao[1‡], Kai Zheng[2‡], Baoyi Guan[3], Mengmeng Guo[4], Lei Song[1], Jie Gao[3], Hua Qu[3], Yuhui Wang[4], Dazhuo Shi[3,*] and Ying Zhang[3,*]

[1] Department of Graduate School, Beijing University of Chinese Medicine, Beijing, China

[2] School of Computer Science and Engineering, Central South University, Changsha, China

[3] National Clinical Research Center for Chinese Medicine Cardiology, Xiyuan Hospital, China Academy of Chinese Medical Sciences, Beijing, China

[4] Institute of Cardiovascular Sciences, Health Science Center, Peking University, Key laboratory of Molecular Cardiovascular Sciences, Ministry of Education, Beijing, China

‡ These authors contribute equally to this work.

*Correspondence should be addressed to:

Dazhuo Shi and Ying Zhang, Cardiovascular Diseases Center, Xiyuan Hospital, China Academy of Chinese Medical Sciences, Beijing, China.

E-mail addresses: shidztcm@163.com (D.Z. Shi) and echo993272@sina.com (Y. Zhang)

Abstract

Background: Drug repositioning, the strategy of unveiling novel targets of existing drugs could reduce costs and accelerate the pace of drug development. To elucidate the novel molecular mechanism of known drugs, considering the long time and high cost of experimental determination, the efficient and feasible computational methods to predict the potential associations between drugs and targets are of great aid.

Methods: A novel calculation model for drug-target interaction (DTI) prediction based on network representation learning and convolutional neural networks, called DLDTI，was generated. The proposed approach simultaneously fuses the topology of complex networks and diverse information from heterogeneous data sources, and copes with the noisy, incomplete, and high-dimensional nature of large-scale biological data by learning the low-dimensional and rich depth features of drugs and proteins. The low-dimensional feature vectors were used to train DLDTI to obtain the optimal mapping space and to infer new DTIs by ranking candidates according to their proximity to the optimal mapping space. More specifically, based on the results from the DLDTI, we experimentally validate the predicted targets of tetramethylpyrazine (TMPZ) on atherosclerosis progression *in vivo*.

Results: The experimental results show that the DLDTI model achieves promising performance under 5-fold cross-validations with AUC values of 0.9172, which is higher than the methods using different classifiers or different feature combination methods mentioned in this paper. For the validation study of TMPZ on atherosclerosis, a total of 288 targets were identified and 190 of them were involved in platelet activation. The pathway analysis indicated signaling pathways, namely PI3K/Akt, cAMP and calcium pathways might be the potential targets. Effects and molecular mechanism of TMPZ on atherosclerosis were experimentally confirmed in animal models.

Conclusions: DLDTI model can serve as a useful tool to provide promising DTI candidates for experimental validation. Based on the predicted results of DLDTI model, we found TMPZ could attenuate atherosclerosis by inhibiting signal transductions in platelets. The source code and datasets explored in this work are available at https://github.com/CUMTzackGit/DLDTI.

Keywords: drug-target interaction; heterogeneous information; network representation learning; stacked auto-encoder; deep convolutional neural networks; atherosclerosis

Background

Research on drug development is becoming increasingly expensive, while the number of newly approved drugs per year remains quite low [1] [2]. In contrast to the classical hypothesis of “one gene, one drug, one disease”, drug repositioning aims to identify new characteristics of existing drugs [3]. Considering the available data on safety of already-licensed drugs, this approach could be advantageous compared with traditional drug discovery, which involves extensive preclinical and clinical studies [4]. Currently, a number of existing drugs have been successfully tuned to the new requirements. Methotrexate, an original cancer therapy, has been used for the treatment of rheumatoid arthritis and psoriasis for decades [5]. Galanthamine, an acetylcholinesterase inhibitor for treating paralysis, has been approved for Alzheimer’s disease [6].

Besides the evidence based on biological experiments and clinical trials, computational methods could facilitate high-throughput identification of novel target proteins of known drugs. To discover targets of drugs with known chemical structures, the prediction of drug-target interaction (DTI) based on numerous computational approaches have provided an alternative to costly and time-consuming experimental approaches [7]. In the past years, DTI prediction has bolstered the identification of putative new targets of existing drugs [8]. For instance, the computational pipeline predicted that telmisartan, an angiotensin II receptor antagonist, had the potential of inhibiting cyclooxygenase. *In vitro* experimental evidence also validated the predicted targets of this known drug [9]. Further, combined with *in silico* prediction, *in vitro* validation and animal phenotype model demonstrated that, topotecan, a topoisomerase inhibitor also had the potential to act as a direct inhibitor of human retinoic-acid-receptor-related orphan receptor-gamma t (ROR-γt) [10].

Most existing prediction methods mainly extract information from complex networks. Bleakley et al. [11] proposed a support vector machine-based method for identifying DTI based on bipartite local model (BLM). Mei et al. [12] proposed BLMNII method

for predicting DTIs based on the bipartite local model and neighbor-based interaction-profile inference. In addition, some researchers adopted kernelized Bayesian matrix factorization to predict DTIs, called KBMF2K [13]. A key step of KBMF2K is utilizing dimensional reduction, matrix factorization, and binary classification. Although homogenous network-based derivation methods have achieved good results, they are less effective in low-connectivity (degree) drugs for known target networks. The introduction of heterogeneous information can provide more perspective for predicting the potential of DTI. Recently, Luo et al. proposed a heterogeneous network-based unsupervised method for computing the interaction score between drugs and targets, called DTInet [9]. Subsequently, they proposed a neural network-based method [14] for improving the prediction performance of DTI. Effective integration of large-scale heterogeneous data sources is crucial in academia and industry.

Tetramethylpyrazine (TMPZ) is a member of pyrazines derived from *Rhizoma Chuanxiong* [15]. According to a recent review, TMPZ could attenuate atherosclerosis by suppressing lipid accumulation in macrophages [16], alleviation of lipid metabolism disorder [17], and attenuation of oxidative stress [18]. However, since atherosclerosis is a chronic illness involving multiple cells and cytokines [19], besides lipoprotein metabolism and oxidative stress, other possible targets of TMPZ on atherosclerosis remain unexplored.

In this study, a novel model for prediction of DTI based on network representation learning and convolutional neural networks, referred to as DLDTI is presented for *in silico* identification of target proteins of known drugs. New DTIs were inferred by integrating drug- and protein-related multiple networks, to demonstrate the DLDTI's ability of integrating heterogeneous information and neural networks to extract deep features of drugs and target networks as well as attributes to effectively improve prediction accuracy. Moreover, comprehensive testing demonstrated that DLDTI could achieve substantial improvements in performance over other prediction methods.

Based on the results predicted by DTDTI, new interactions between TMPZ and targets involved in atherosclerosis, namely signal transduction in platelets, were validated *in vivo*. The anti-atherosclerosis effect of TMPZ was confirmed in a novel atherosclerosis model. In summary, these improvements could advance studies on drug-target interaction.

Methods

Prediction experiments

Human drug-target interactions database

In this study, we use the DrugBank established by Wishart *et al.* as the benchmark dataset, which can be downloaded at http://www.drugbank.ca [20]. The chemical structure of each drug in SMILES format is extracted from and extracted from DrugBank. In the experiments, only those that satisfied the human target represented by a unique EnsemblProt login number were used. In detail, 904 drugs and 613 unique human targets (proteins) were linked to construct a DTI network A as positive samples, and a matching number of unknown drug-target pairs (by excluding all known DTIs) were randomly selected as negative samples.

Feature representation

Gaussian interaction profile kernel similarity for drugs and targets. On the basis of previous work, drug similarity can be measured by calculating nuclear similarity through Gaussian interaction profile (GIP) kernel similarity [21][22]. The GIP similarity between drug d_i and drug d_j is defined as follow:

$$\mathrm{D}_{sim}(d_i, d_j) = exp\left(-\tau_d * \left|\left|V(d_i) - V(d_j)\right|\right|^2\right) \quad (1)$$

where the binary vector $V(d_i)$ and $V(d_j)$ is the i-th row vector and the j-th row vector of the drug-target interaction network A. The parameter τ_d is the kernel bandwidth. It computes by normalizing original parameter τ_d':

$$\tau_d = \frac{\tau'_d}{\frac{1}{n_d}\sum_{i=1}^{n_d}\left||V(d_i)|\right|^2} \quad (2)$$

131 Similarly, the GIP similarity for targets can be defined as follows:

$$\mathrm{D}_{sim}(d_i, d_j) = exp\left(-\tau_d * \left|\left|V(p_i) - V(p_j)\right|\right|^2\right) \quad (3)$$

132 where the binary vector $V(p_i)$ and $V(p_j)$ is the *i*-th row vector and the *j*-th column
133 vector of the drug-target interaction network A. The parameter τ_p is the kernel
134 bandwidth. It computes by normalizing original parameter $\tau_p{}'$:

$$\tau_p = \frac{\tau'_p}{\frac{1}{n_p}\sum_{i=1}^{n_p}\left||V(p_i)|\right|^2} \quad (4)$$

135 **Protein sequence feature.** The sequences for drug targets (proteins) in *Homo sapiens*
136 downloaded from the String database (http://string-db.org/)[23]. The *k-mer* algorithm
137 is used to count Subsequence information in protein sequences and uses it as a feature
138 vector to solve the alignment problem posed by differences in sequence length [24].

139 **Drug structure feature.** The SMILES for drugs downloaded from the DrugBank
140 database. We use Morgan fingerprint, a circular fingerprint, to map the structure
141 information of drugs to feature vectors.

142 **Graph embedding-based feature for drugs and targets**. Graph data is rich in
143 behavioral information about nodes, and behavioral information can be used as a
144 descriptor to describe drugs and targets that can be more comprehensive description
145 of the characteristics [25]. So how do we map a high-dimensional dense matrix like
146 graph data to a low-density vector? Here we introduce the Graph Factorization
147 algorithm [26]. Graph factorization (GF) is a method for graph embedding with time
148 complexity O(|E|). To obtain the embedding, GF factorizes the adjacency matrix of
149 the graph to minimize the loss functions as follow:

$$\varepsilon(P,Q,\lambda)=\frac{1}{2}\sum_{(i,j)\in E}(P_{ij}-<Q_i,Q_j>)^2+\frac{\lambda}{2}\sum_i\left||Q_i|\right|^2 \quad (5)$$

where λ is the regularization coefficient. P and Q are the adjacency matrix with weights and factor matrix, respectively. E is the set of edges, which includes *i* and *j*.

The gradient of the function ε with respect to Q_i is defined as follow:

$$\frac{\partial\varepsilon}{\partial Q_i}=-\sum_{k\in N_o}\left(P_{ij}-<Q_i,Q_j>\right)Q_j+\lambda\,Q_i \quad (6)$$

where N_o is the set of neighbors of node o. With the Graph Factorization algorithm, graph embeddings of drugs and targets in the drug-target interaction network can be obtained to describe their behavioral information.

Stacked Autoencoder

As DLDTI integrates heterogeneous data from multiple sources, including protein sequence information, drug structure information, and drug-target interaction network information, the integrated biological data suffers from noise, incomplete and high-dimensional. Here, the stack autoencoder (SAE) is introduced to find the optimal mapping of drug space to target space to obtain low dimensional drug Feature vector [27][28]. SAE can be defined as follows:

$$y=f(x)=S_e(W+b) \quad (7)$$

$$z=g(y)=S_d(W'y+b') \quad (8)$$

Where y and z are encoding function and decoding function respectively. W and W' are the relational parameters between two layers. b and b' are vectors of bias parameters. The activation function used is ReLU:

$$S_e(t)=S_d(t)=max(0,W^T+b) \quad (9)$$

Convolutional neural network

Lecun *et al*. proposed convolutional neural networks in 1989[29]. Subsequently, they have performed well in tasks such as image classification, sentence classification, and biological data analysis. Thus, in this study, convolutional neural networks were used to train supervised learning models to predict potential DTIs. In this work, convolutional neural networks were chosen as supervised learning models to learn deep features and predict potential DTIs. The model used includes convolutional and activation layers, a Maxpooling layer, a fully connected layer and a softmax layer. Their roles are, respectively, to extract depth features, down-sample, and classify samples. The convolutional layer is one of the most important parts of the CNN and aims to learn the deep characteristics of the input vectors, which is defined as follows

$$C_m = \sum_{i=1}^{N_k} W_i X_{m+j} \tag{10}$$

where X is the input feature of length L. N_k is the number of kernels. $m \in \{0, \ldots, L-N\}$, W is a weight vector of length N_k. Then, the feature map C_m is put into the activation function ReLU, which is defined as follow:

$$f(x) = max(0, x) \tag{11}$$

The role of the ReLU function is to increase the nonlinear relationship between the layers of the neural network, save computation, solve the gradient disappearance problem, and reduce the interdependence of parameters to mitigate the overfitting problem.

The convolutional and maximum pooling layers can extract important features from the input vectors. The output of all kernels is then concatenated into a vector and fed to the fully-connected layer $f(W \cdot y)$. Where y is the output of Maxpooling layer and W is the weight matrix. Finally, the softmax layer scores the input vectors as a percentage.

Pathway analysis of predicted results from DLDTI

Atherosclerosis-related gene sets were collected from GeneCards (https://www.genecards.org/) [30]. After using retrieve tool on Uniprot database (https://www.uniprot.org/), different identifiers from Drug Bank and GeneCards were converted to UniProtKB. Based the intersection of potential targets of TMPZ from DLDTI model and confirmed target proteins of atherosclerosis, the matched targets were regarded as the predicted targets of TMPZ on atherosclerosis. The predicted targets were uploaded to the Search Tool for the Retrieval of Interacting Genes/Proteins database (STRING, Version 11) (https://string-db.org/) [23] for Kyoto Encyclopedia of Genes and Genomes (KEGG) pathway and Gene Ontology (GO) biological process analysis.

Validation experiments

Ldlr-/- hamsters

This study was approved by the Animal Ethics Committee of Xiyuan Hospital and strictly adhered to the principles of laboratory animal care (NIH publication No.85Y23, revised 1996). Male, 8-week aged and low-density lipoprotein receptor knock-out (Ldlr-/-) hamsters were provided by the health science center, Peking University. The Ldlr-/- genotype was confirmed using polymerase chain reaction (PCR) analysis of DNA extracts from ears [31]. After one week of acclimatization, they were fed on high-cholesterol and high-fat (HCHF) diet containing 15% lard and 0.5% cholesterol (Biotech company, China) for eight weeks. The Ldlr-/- hamsters were then randomly divided into three groups according to their weights (n=8 per group) and orally administered with a mixture of volume vehicle (distilled water), TMPZ (32mg/kg/d) and clopidogrel (32mg/kg/d) drugs for eight weeks. Wild type (WT) golden Syrian hamsters (n=8) purchased from Vital River Laboratory (Charles River, Beijing, China) were fed on a standard chow diet as healthy control. All hamsters were maintained on a 12-hour light/12-hour dark cycle with free access to

water.

Hamsters were fasted for 12h and anesthetized by intraperitoneal injection of 1% sodium phenobarbital (70mg/kg). Blood samples were taken from abdominal aortas and plasma was separated by centrifugation for 10 min at 2700×g. TC, TG and HDL were determined using commercially available kits (BIOSINO, China)

Oil red O staining

As described previously[32], anesthetized hamsters were perfused with 0.01M PBS through the left ventricle. In brief, hearts and whole aortas were placed in 4% paraformaldehyde solution overnight, transferred to 20% sucrose solution for one week. Hearts were then fixed into O.C.T compound and cross-sectioned (8μm per slice). The atherosclerotic lesions in aortic root were stained with 0.3% Oil red O solution (Solarbio, China), rinsed with 60% isopropanol and distilled water and counterstained with hematoxylin. The results were represented by the percentage positive area of total area (*en face* analysis) and net lesion area (aortic root sections). Images were analyzed with Image J[33].

Histological analysis

Analysis of atherosclerotic plaque cell composition was determined by immunohistochemistry (IHC) analysis of the aortic root. Macrophages and smooth muscle cells (SMC) were stained with CD68 (BOSTER, BA36381:100) antibody and a-SMA antibody (BOSTER, A03744, 1:100) as reported previously in hamster researches[31]. Then biotinylated second antibody (Vector Laboratories, ABC Vectastain, 1:200) were used for incubation under 2% normal blocking serum. The cryosections were visualized using 3,3-diaminobenzidine (Vector Laboratories, DAB Vectastain). The results were represented by the percentage positive area of total cross-sectional vessel wall area in the aortic root sections and analyzed using Image J[33].

Washed platelet preparation

243 Blood per hamster, 3 to 4 mL was collected from abdominal aortas into a tube
244 containing an acid-citrate-dextrose anticoagulant (83.2mM D-glucose, 85mM
245 trisodium citrate dihydrate, 19mM citric acid monohydrate, pH5.5). Platelet-rich
246 plasma (PRP) was prepared after centrifugation at 300×g for 10min in room
247 temperature. For washed platelet preparation, PRP was centrifuged at 1500×g for
248 2min. After collecting supernatant consisting of platelet-poor plasma into another
249 centrifuge tube, the remaining PRP was washing three times, and the pellet was
250 re-suspended in a modified Tyrode buffer (2.4mM HEPES, 6.1mM D-glucose,
251 137mM NaCl, 12mM HaHCO3, 2.6mM KCl, pH7.4).

252 **Assessment of platelet activity**

253 Washed platelets were loaded with fura-2/AM(5μM, Molecular Probe) in the presence
254 of Pluronic F-127 (0.2μg/mL, Molecular Probe) and then incubated at 37℃ for 1
255 hour in the dark [34]. Platelets were washed and re-suspended in Tyrode buffer
256 containing 1mM calcium. After activation of ADP (20μM, Sigma), intracellular
257 calcium concentration was measured using a fluorescence mode of Synergy H1
258 microplate reader (Biotek, USA). Excitation wavelengths was alternated at 340 and
259 380 nm. Excitation was measured at 510 nm. TritonX-100 and EGTA were used for
260 calibration of maximal and minimal calcium concentrations, respectively. Washed
261 platelets were activated by ADP and then lysed by 0.1M HCl on ice. According to the
262 manufacturer's instructions, the level of intracellular cAMP was determined by
263 ELISA (Enzo Life Sciences, ADI-900-066).

264 **Western blot analysis**

265 Washed platelets from each group were lysed with radioimmunoprecipitation assay
266 buffer with the presence of protease and phosphatase inhibitor mixtures on ice
267 (Solarbio, China). Lysates were separated by 10000×g centrifugation for 10 min at
268 4℃. Total protein concentrations were determined by BCA method. Equal amounts
269 of total protein (40μg) were resolved in SDS-PAGE and electroblotted. The

nitrocellulose membranes were blocked with 5% skimmed milk at room temperature for 2 hours and incubated with primary antibodies targeting PI3K(CST, 4257T, 1:500), Akt(CST, 9272, 1:2000), p-Akt(CST,2965,1:1000) and GADPH (Abcam, ab8245, 1:5000) overnight at 4℃. The membranes were then incubated with the HRP-conjugated anti-rabbit antibody for 1 hour at 37℃, followed by enhanced chemiluminescence detection.

Statistical analysis

All data were expressed as mean ±standard error. Shapiro-Wild test and Levene's test were used for normality of data distribution and homogeneity of variances, respectively. An unpaired student's t-test were used to compare data in different groups when data normally distributed and variances were equal among groups. Unpaired t test with Welch's correction were used when unequal standard deviation among groups. Mann-Whitney test were used for nonparametric test. All *p*-values less than 0.05 were considered statistically significant. All statistical analyses were performed using GraphPad Prism 8.0 (GraphPad, United states).

Results

Overview of DLDTI and performance evaluation on predicting drug-target interaction

A new computational model referred to as DLDTI was developed to predict potential DTIs to identify novel behavior of traditional drugs based on complex networks and heterogeneous information. As an overview (Figure 1), DLDTI integrates learning from complex network's various heterogeneous information to obtain low-dimensional and deep rich features (Figure 2), through a processing method known as compact feature learning. During compact feature learning, the resulting low-dimensional descriptor integrates attribute characteristics, interaction information, relational properties, and network topology of each protein or target node in the complex network. DLDTI then determines the optimal mapping from the plenary

297 mapping space to the prediction subspace, and whether the feature vector is close to
298 the known correlations. Afterwards, DLDTI infers the new DTIs by ranking the DTI
299 candidates according to their proximity to the predicted subspace.

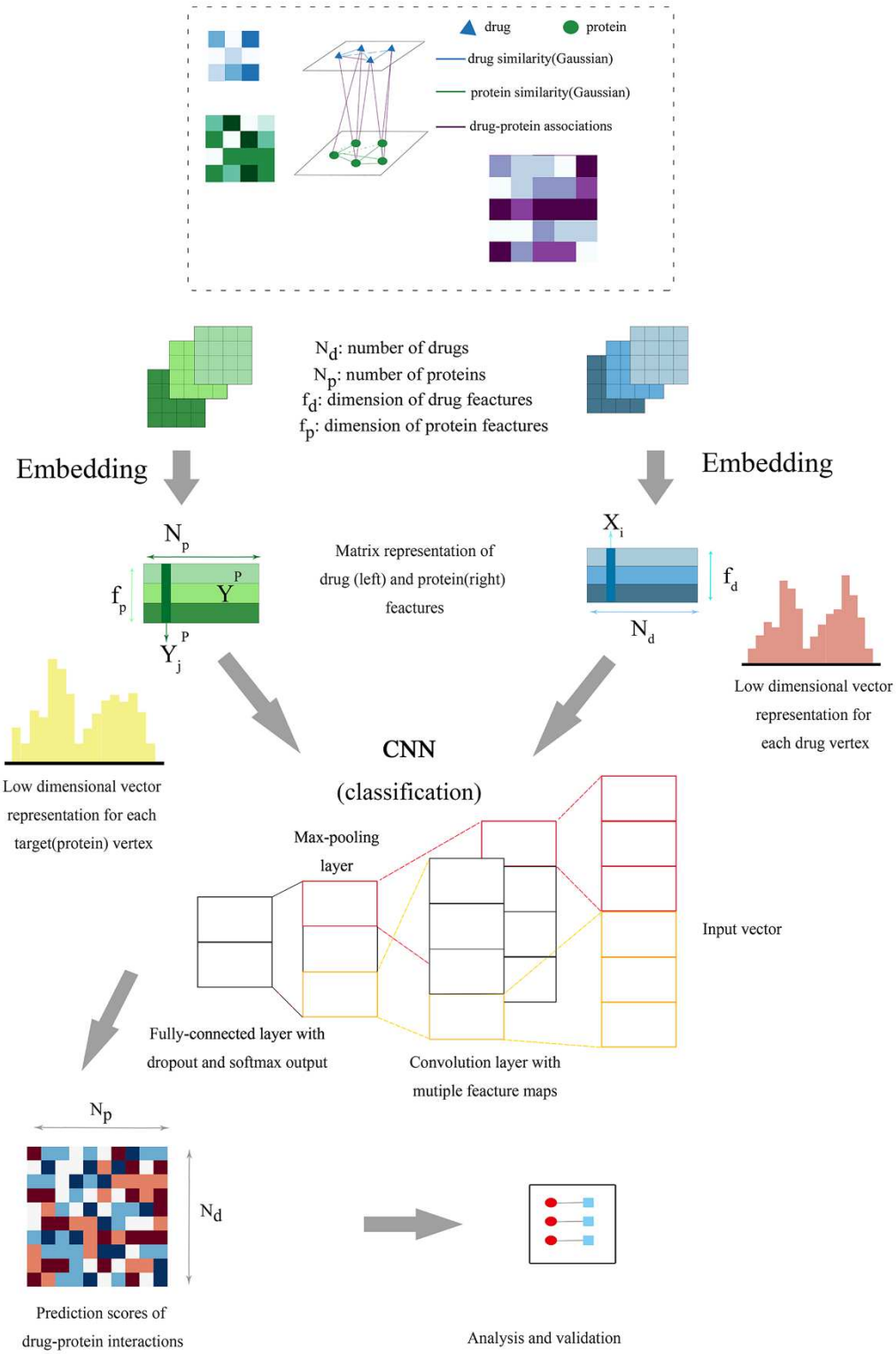

300

Figure 1. The flowchart of the DLDTI pipeline. DLDTI first integrates a variety of drug-related information sources to construct a heterogeneous network and applies a compact feature learning algorithm to obtain a low-dimensional vector representation of the features describing the topological properties for each node. Next, DLDTI determines the optimal mapping from the plenary mapping space to the prediction subspace, and whether the feature vector is close to the known correlations. Afterwards, DLDTI infers the new DTIs by ranking the candidates according to their proximity to the predicted subspace.

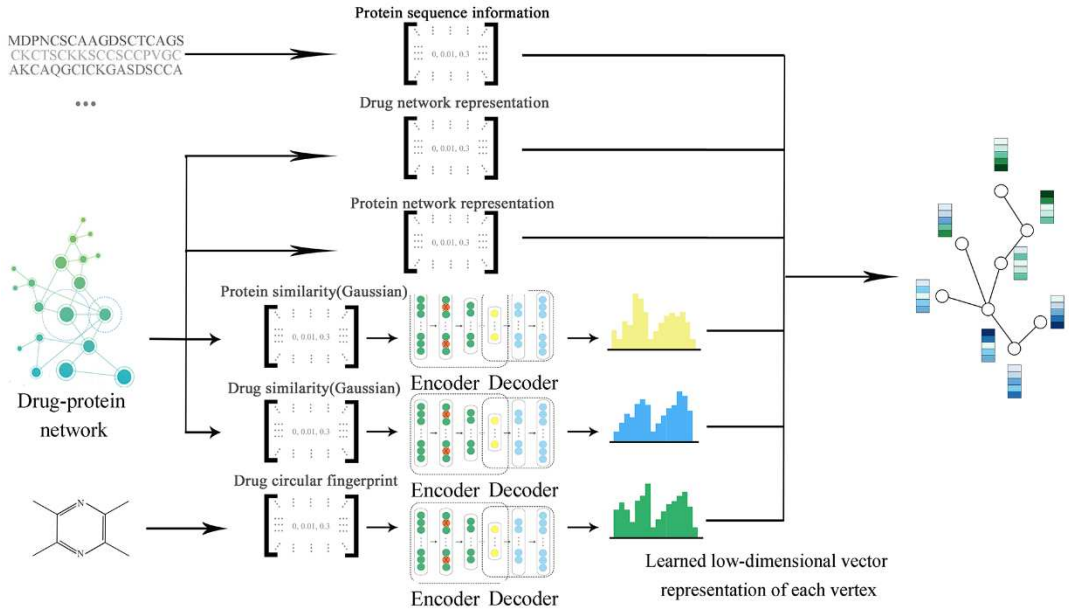

Figure 2. Schematic illustration of compact feature learning. The Node2Vec algorithm is firstly used to calculate the topology information in complex networks. GIP kernel similarity and drug structure information are then extracted by a stacked automatic encoder, and the heterogeneous information is integrated to obtain a low-dimensional representation of the feature vector of each node. The resulting low-dimensional descriptor integrates the attribute characteristics, interaction information, relationship attributes and network topology of each protein or target node in the complex network.

DLDTI yields accurate DTI prediction. Firstly, the predictive performance of DLDTI was assessed using five-fold cross-validation, where randomly selected subset of

one-fifth of the validated DTI were paired with an equal number of randomly sampled non-interacting pairs to derive the test set. The remaining 75% of known DTI and same number of randomly sampled non-interacting pairs were used to train the model. DLDTI was compared with three methods based on different classifiers used for DTI prediction, including DTI-ADA, DTI-KNN, and DTI-RF [35][36][37]. The comparison revealed that DLDTI consistently outperforms the other three methods, with 0.93% higher AUC, 3.55% higher AUPR, 0.61% higher accuracy (Acc), 3.96% higher precision (Pre) than the second-best method (Fig. 3c, Fig. 3d and Fig. 3e). Compared to DTI-ADA (which predicts DTI based on the AdaBoost classifier), the DLDTI of the area under AUROC and AUPR was 6.96% and 7.81% higher, respectively, which could have been due to the inability of traditional machine learning to extract deeper abstract features for prediction, resulting in poor performance, while DLDTI applies a deep convolutional neural network approach and is able to capture the potential structural properties of complex networks and heterogeneous information.

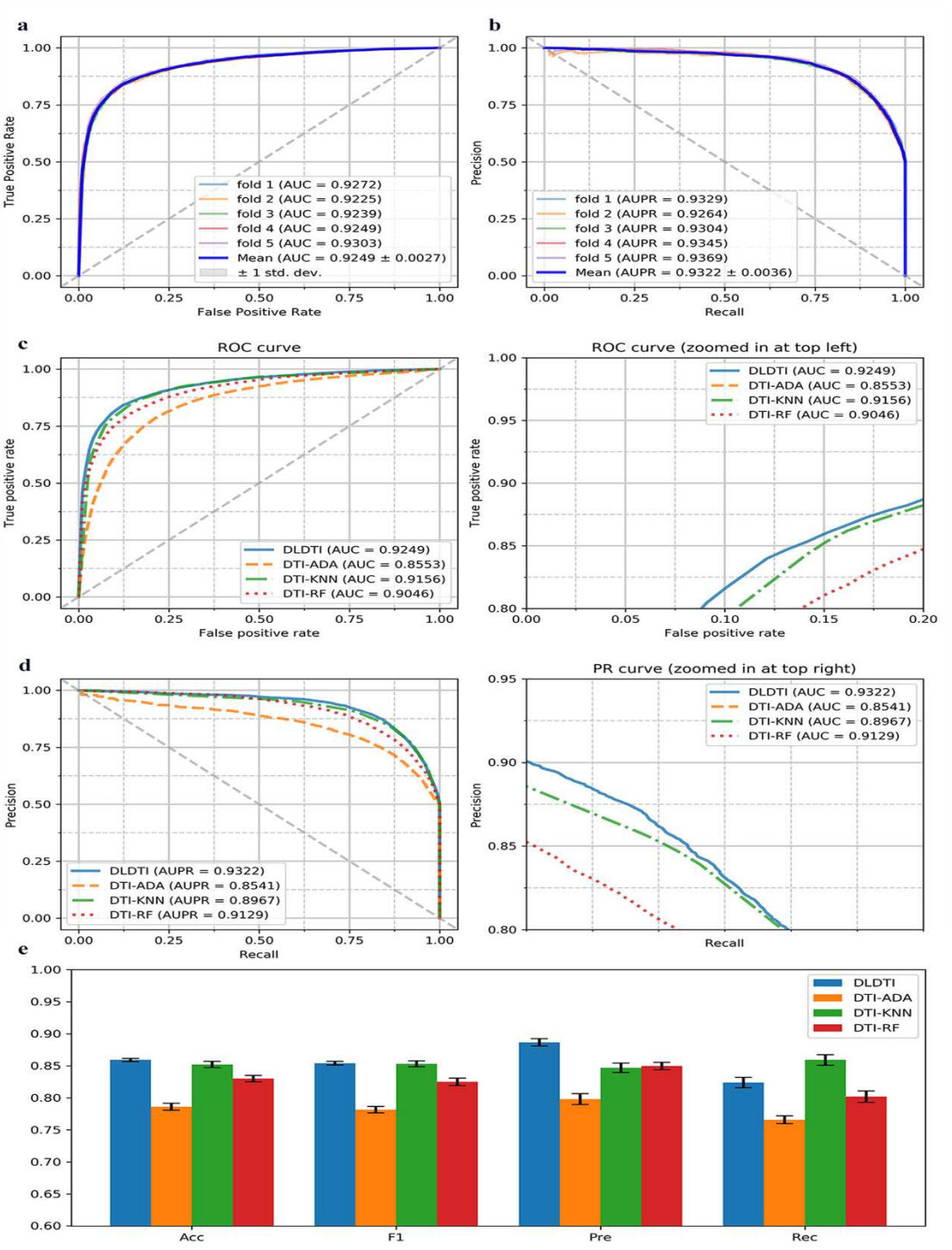

Figure 3. Performance of DLDTI. (a) ROC curves performed by DLDTI model on DrugBank dataset. (b) PR curves performed by DLDTI model on DrugBank dataset. (c) Performance comparison (AUC scores) among four different prediction model which are DTI-ADA, DTI-KNN, and DTI-RF.(d)Performance comparison (AUPR

scores) among four different prediction models including DTI-ADA, DTI-KNN, and DTI-RF.(e)Performance comparison (Acc., F1, Pre., Rec. scores) among DTI-ADA, DTI-KNN, and DTI-RF prediction models.

Enrichment analysis suggested TMPZ might affect signal transduction pathways involved in platelet activation

To elucidate the potential function of TMPZ on atherosclerosis, the predicted results from DLDTI model were uploaded to the search tool for retrieval of interacting genes/proteins database (STRING) to determine over-represented KEGG pathways and GO categories. GO analysis demonstrated that 31.4% of genes were involved in signal transduction (Additional file 1). As shown in Table 1, PI3K/Akt signaling pathway, neuroactive ligand-receptor interaction, MAPK signaling pathway, calcium signaling pathway, Rap1 signaling pathway, cGMP-PKG signaling pathway, and cAMP signaling pathway were the top-ranked results of KEGG enrichment. It is noteworthy that ADP-mediated platelet activation via purinergic receptors included almost all signal transduction pathways shown in Table 1 [38][39]. Interestingly, among the 288 predicted targets of TMPZ on atherosclerosis, 190 proteins were also involved in the platelet activation process (Additional file 2). Therefore, it was assumed that the anti-atherosclerosis potential of TMPZ could be largely attributed to its inhibition of purinergic receptor-dependent platelet activation, which involves signal transduction pathways such as PI3K/Akt. Based on the predicted result, clopidogrel, an anti-platelet drug widely used in the clinical application, was chosen as the positive control.

Table 1 KEGG pathway enrichment analysis of DLDTI results

Class	KEGG term	Count	*P* value
Signal transduction	PI3K-Akt signaling pathway	36	2.49E-17

	Neuroactive ligand-receptor interaction	32	6.04E-17
	MAPK signaling pathway	29	1.08E-13
	Calcium signaling pathway	26	1.01E-15
	Rap1 signaling pathway	22	2.99E-11
	cGMP-PKG signaling pathway	20	2.99E-11
	cAMP signaling pathway	16	3.83E-07
Metabolism	Metabolism of xenobiotics by cytochrome P450	23	4.27E-20
	Steroid hormone biosynthesis	17	1.28E-14
	Retinol metabolism	15	5.89E-12
Immune system	Complement and coagulation cascades	21	3.06E-17
	Th17 cell differentiation	15	1.77E-09
Others	Regulation of actin cytoskeleton	16	6.90E-07
	Gap junction	15	2.74E-10
	Fluid shear stress and atherosclerosis	15	2.91E-08

Validation

Ldlr-/- hamsters developed severe hyperlipidemia and atherosclerosis lesions when fed with HFHC diet

Before dietary induction, genotypes were determined by PCR analysis. Using ear genomic DNA, 194-nucleotide deletion (Δ194) was detected in homozygous (-/-) hamsters (Figure 4a). After feeding them on HCHF diet for 16 weeks, Ldlr-/- hamsters developed severe hyperlipidemia. As an antiplatelet medication, clopidogrel did not influence circulating levels of TC, TG, HDL and non-HDL (Figure 4b, 4c, 4d and 4e). Compared with vehicle-treated hamsters, decreased levels of TC (p<0.05) and non-HDL (p<0.05) were observed in TMPZ-treated group (Fig. 4b and 4d). However, TMPZ did not influence TG or HDL levels.

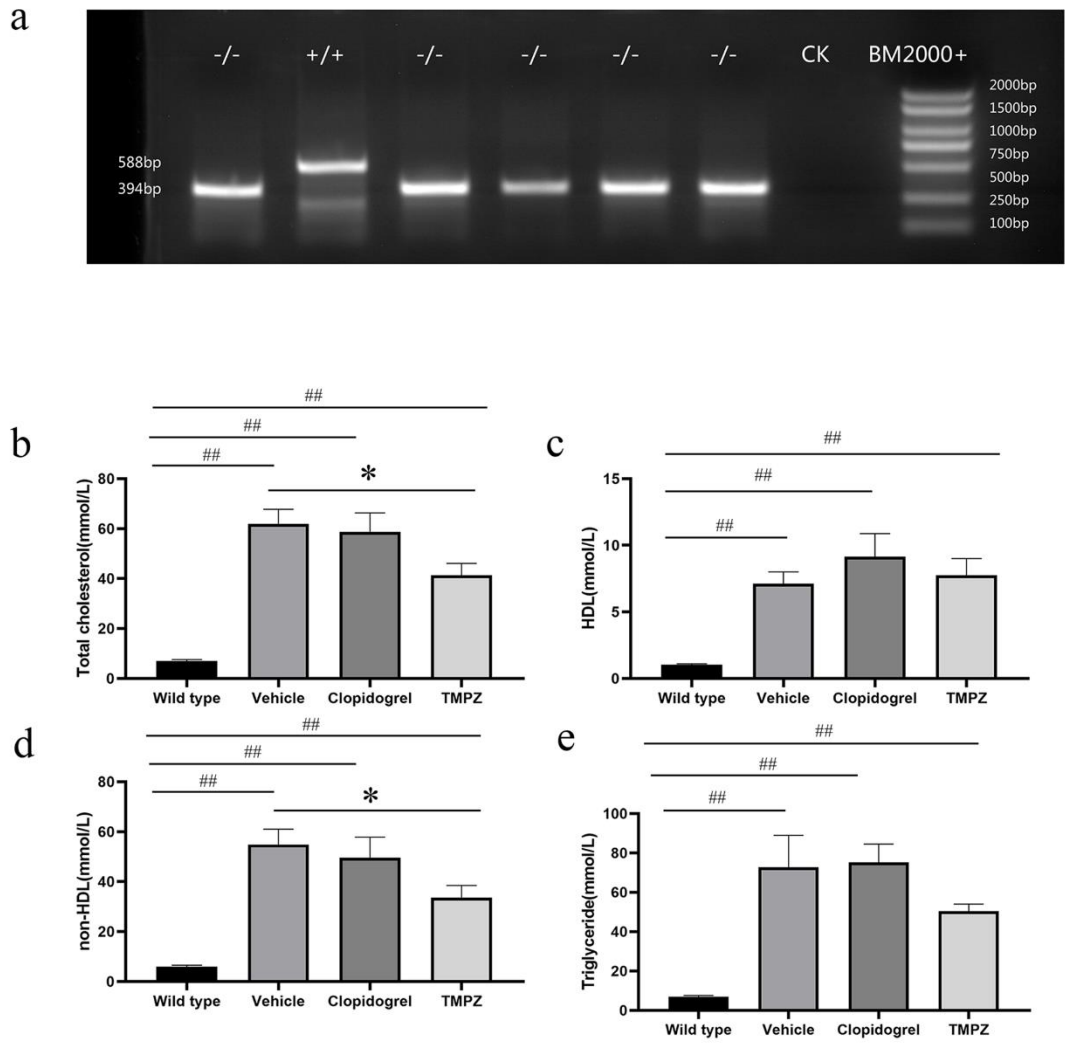

Figure 4. Genotyping and lipid parameters between different groups. (a) PCR analysis was performed using ear genomic DNA from WT (+/+) and homozygote (−/−) with the Δ194 deletion. The concentrations of plasma TC (b), HDL(c), non-HDL(d) and

TG(e) were measured in WT, vehicle, TMPZ and clodipogrel groups at the endpoint of this experiment. Differences were assessed by unpaired student t's test or Mann-Whitney test. * $p<0.05$ versus Vehicle, ** $p<0.01$ versus Vehicle. ## $p<0.01$ versus WT.

TMPZ ameliorated atherosclerosis lesion progression

The *en face* analysis demonstrated that vehicle-treated hamsters developed significant atherosclerotic lesions (mean value 28.38%) throughout the whole aorta. However, atherosclerotic lesions induced by the same dietary manipulation in TMPZ- and clopidogrel-treated groups were significantly decreased (mean value 10.02% and mean value 17.47%, respectively) (Figure 5a and 5b). It's noteworthy that the lesion area in TMPZ-treated group was also less than that in clopidogrel-treated group (Figure 5b). As the blank control group, WT hamsters on chow diet did not develop any lesions throughout the aorta.

Similar to the *en face* analysis, the HFHC fed vehicle group had significantly increased lesion areas (mean area 29.58×10^4 μm^2) in aortic roots compared to the blank controls measured by image analysis of Oil Red O staining, and either TMPZ (mean area 13.25×10^4 μm^2) or clopidogrel (mean area 16.99×10^4 μm^2) treatment reduced the lipid-rich areas (Figure 5c and 5d).

Under the stimulation of adhesion molecules, monocytes infiltrate into the intima and differentiate into macrophages [40]. Besides macrophage accumulation, diminished SMC could also exacerbate the formation of unstable plaques [41]. To determine the components of atherosclerosis lesions in the aortic root, IHC staining for macrophages and SMC was performed. As shown in Figure 5e and 5f, the percentage of macrophage positive staining in lesions was increased by atherosclerosis progression in the vehicle-treated group. WT group (mean value 1.48%) had significantly fewer macrophage accumulation than vehicle-treated group (mean value 6.65%). Infiltrated macrophages in lesions were significantly decreased by TMPZ

(mean value 2.52%) or clopidogrel (mean value 3.07%) treatment. As shown in Figure 5g and 5h, the percentage of a-SMA positive staining was diminished in Ldlr-/- hamsters (mean value 9.27%) compared with the WT hamsters (mean value 16.76%). Administration TMPZ (mean value 16.50%) or clopidogrel (mean value 16.09%) for 8 weeks could ameliorate SMC reduction in atherosclerosis lesions.

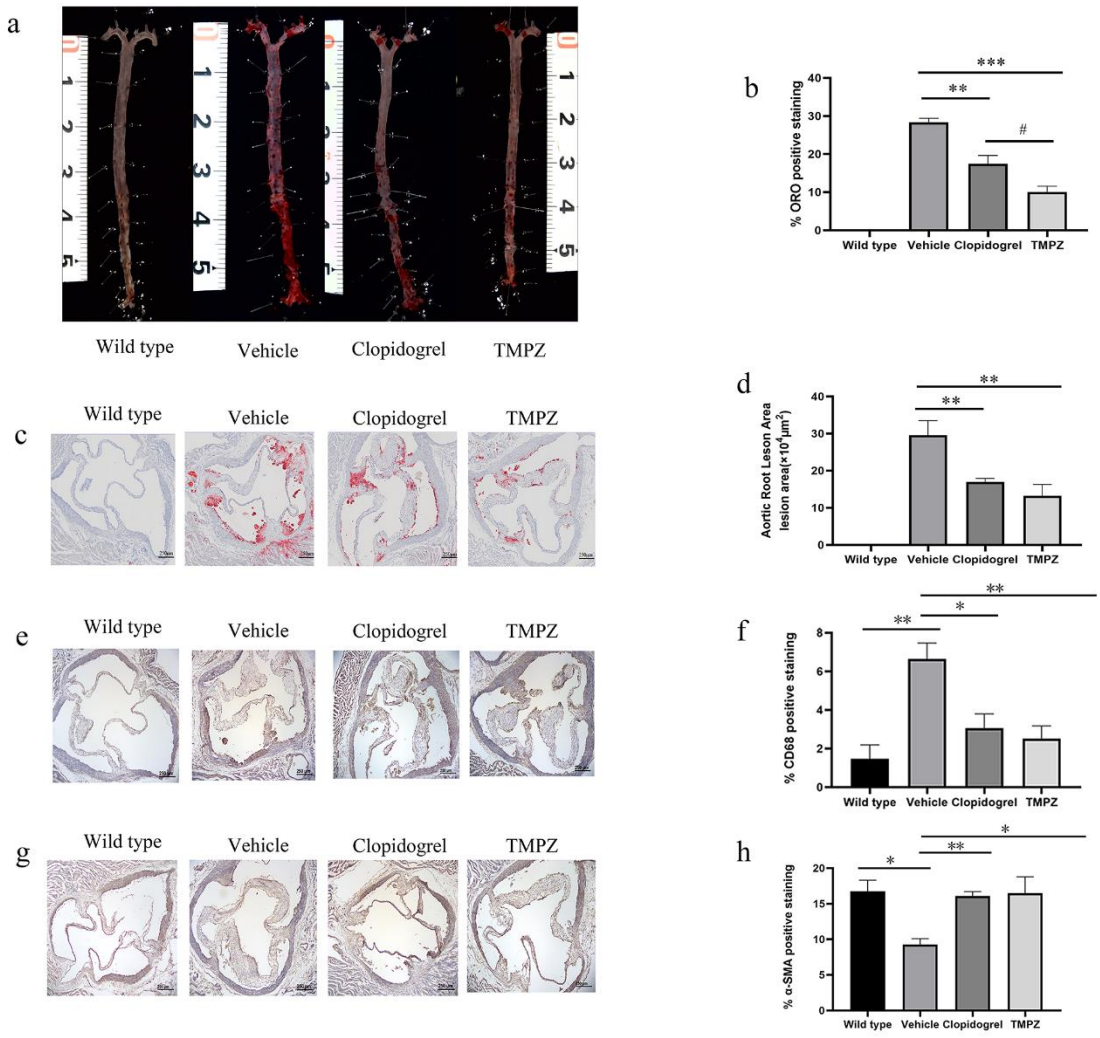

Figure 5. Histological analysis. (a) Representative images of *en face* analysis. n=6. (b) Quantitative analysis of lesion areas in whole aortas. Differences were assessed by unpaired student t's test. (c) Representative images of Oil Red O staining of aortic root sections. (d) Quantitative analysis of lesion areas in aortic root sections. (e) Representative images of macrophage (CD68) analysis (b) Quantitative analysis of lesions area in macrophage analysis. (f) Representative images of SMC (SMA)

analysis (g) Quantitative analysis of lesions area in SMC. Differences were assessed by unpaired student t's test. * $p<0.05$ versus Vehicle, ** $p<0.01$ versus Vehicle. # $p<0.05$ versus clopidogrel. Scale bar=250μm. n=3.

TMPZ inhibited signaling transduction in ADP-mediated platelet activation

In addition to the surrogates of platelet activation, calcium and cAMP signaling are also essential in signal transduction. Downstream from Gq signaling, protein kinase C activation results in the formation of inositol triphosphate, which leads to an elevation of intracellular calcium [38]. Calcium mobilization is also required for the phosphorylation of Akt (also known as protein kinase B) in PI3K/Akt signaling pathway [42]. In response to ADP, Gi signaling activation mediates the inhibition of AC, resulting in the diminished synthesis of cAMP. The inhibitory effect of Gi on cAMP synthesis could cause platelet activation [39].

Figure 6 shows that fura-2/AM is a membrane-permeant calcium indicator. The ratio of F340/F380 is directly correlated to the amount of intracellular calcium. The data revealed that TMPZ and clopidogrel markedly inhibited calcium mobilization, as detected using fluorescence mode of Synergy H1 microplate reader. Moreover, TMPZ-and clopidogrel-treated groups showed a higher concentration of cAMP in the active platelets. These findings indicate that TMPZ and clopidogrel could inhibit calcium mobilization and elevate intracellular concentration of cAMP, thereby inhibiting platelet activation.

As the major downstream effector of PI3K, Akt plays an essential role in the regulation of platelet activation. Stimulation of platelets with ADP could result in Akt activation, which was indicated by Akt phosphorylation [42]. The protein expressions of PI3K, Akt, and p-Akt in the top-ranked signal transduction pathway were measured to validate the predicted pathways. ADP-induced P2Y12 receptor activation could cause PI3K dependent Akt phosphorylation, a critical positive regulator pathway for signal amplification. There was no difference in PI3K expression levels between WT,

vehicle, TMPZ, and clopidogrel groups (Figure 6c). Phosphorylation of Akt was inhibited by TMPZ or clopidogrel administration when compared with vehicle-treated group. It is noteworthy that phosphorylation of Akt did not differ between WT, TMPZ and clopidogrel groups, which indicates that platelet activity in atherosclerosis hamsters treated with TMPZ or clopidogrel could be comparable to that in healthy ones (Figure 6d). These findings indicate that TMPZ and clopidogrel could attenuate Akt signaling, thereby blocking the platelet activation induced by ADP.

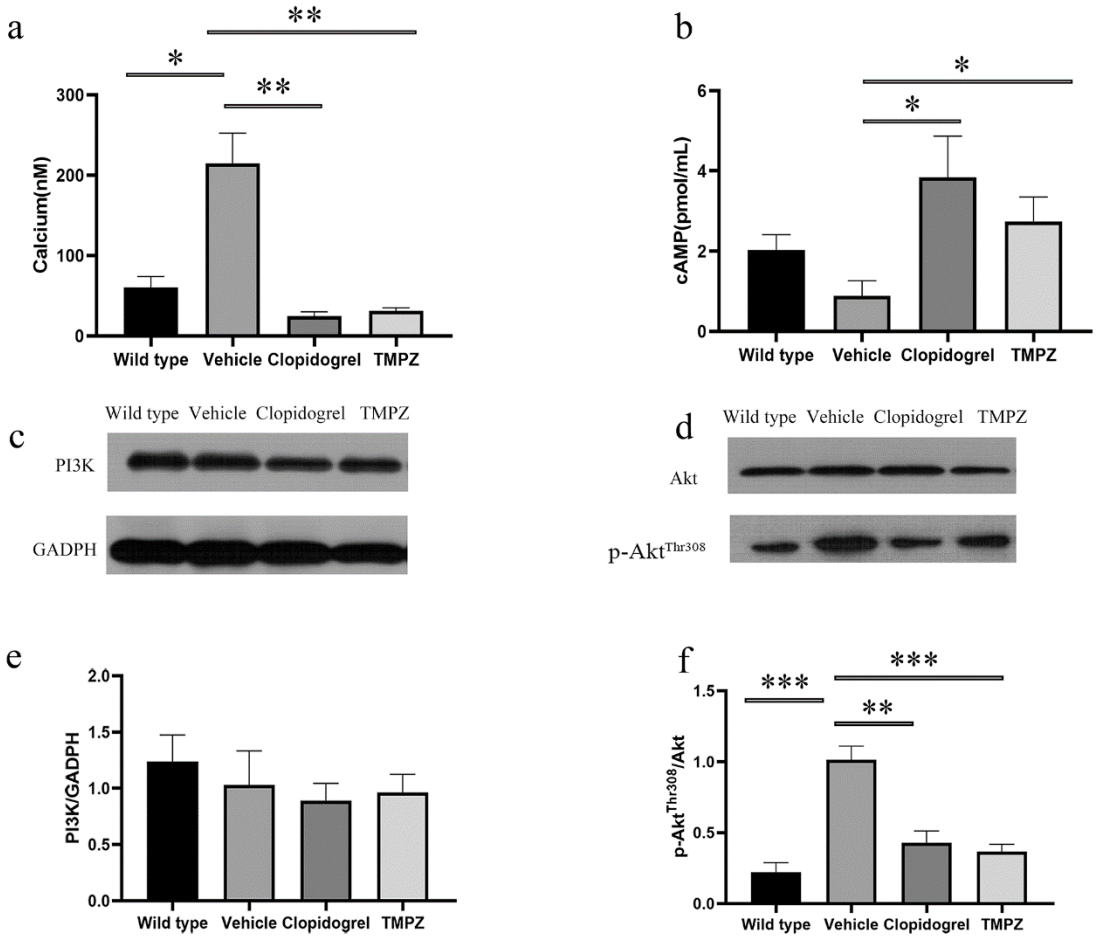

Figure 6. Signaling transduction in ADP-mediated platelet activation. (a) Intracellular calcium concentration. (b) Intracellular cAMP concentration. Western blot analyses of the expression of PI3K (c), Akt (d) and p-Akt (d). Differences were assessed by unpaired student t's test with or without Welch's corrections. ** $p<0.01$ versus Vehicle, * $p<0.05$ versus Vehicle. n=4-6.

Discussion

In summary, we provide a novel DTI model and validate its efficacy in animal model. This DLDTI model could provide an alternate to the high-throughput screening of drug targets. The proposed approach simultaneously fuses the topology of complex networks and diverse information from heterogeneous data sources, and copes with the noisy, incomplete, and high-dimensional nature of large-scale biological data by learning the low-dimensional and rich depth features of drugs and proteins. The low-dimensional descriptors learned by DLDTI that capture attribute characteristics, interaction information, relational properties, and network topology attributes for each drug or target node in a complex network. The low-dimensional feature vectors were used to train DLDTI to obtain the optimal mapping space and to infer new DTIs by ranking potential DTIs according to their proximity to the optimal mapping space. We inferred new DTIs by integrating drug- and protein-related multiple networks, demonstrating the DLDTI's ability to integrate heterogeneous information and that deep neural networks are capable of extracting drug and target networks and the deep features of attributes can effectively improve the prediction accuracy. Compared with three methods based on different classifiers used for DTI prediction, including DTI-ADA, DTI-KNN, and DTI-RF [35][36][37], DLDTI consistently outperforms the other three methods. More importantly, compared to DTI-ADA, the AUROC and AUPR of DLDTI was 6.96% and 7.81% higher. This result could be attributed to the inability of traditional machine learning to extract deeper abstract features for prediction, resulting in poor performance, while DLDTI applies a deep convolutional neural network approach and is able to capture the potential structural properties of complex networks and heterogeneous information.

Furthermore, in the validation study of the DLDTI model, we used TMPZ (a drug with known structure) to explore its effects on atherosclerosis *in vivo*. Consistent with previous studies [16][17][18], the results revealed that TMPZ could ameliorate the phenotyping of atherosclerosis in Ldlr-/- hamsters, a novel atherosclerosis model

[31][43]. Diminished lipid deposition and macrophage accumulation, and increased percentage of SMC were observed in TMPZ- and clopidogrel-treated hamsters. Interestingly, the majority of potential pathways of TMPZ on atherosclerosis were involved in signal transduction of platelet activation. From the initial endothelial dysfunction in the early stage to the destabilized plaques in the advanced stage, platelet plays a pivotal role [44]. Activated platelets act as the key trigger for rupture-prone plaque formation. Current evidence shows that platelet hyperactivity is associated with a prothrombotic state and increased incidence of recurrent cardiovascular events among patients with coronary artery disease [45]. Platelets can be activated by various stimuli like collagen, thrombin, and ADP. Based on the pathway analysis of predicted results, this work focused on signal transduction in ADP-mediated platelet activation (Table 1). The results revealed that the activated signal transductions, characterized by increased calcium mobilization, decreased cAMP concentration and increased phosphorylation of Akt were observed in *ex vivo* platelets from vehicle-treated hamsters, while platelets from TMPZ- and clopidogrel-treated hamsters showed inhibited platelet activation.

A future direction of our study is to solve the “cold-start” problem, which is a challenge that all algorithms that apply collaborative filtering technology will face. In this paper, the top three feature vectors with the highest scores are weighted by 60%, 30%, and 10%, respectively, based on the similarity of protein sequences and the similarity of drug structures, to obtain new interaction feature vectors to solve the cold start problem. In addition, in the validation study, we only examined the top-ranked pathways of signal transduction involved in platelet activation, although reduced TC and non-HDL levels and diminished macrophage accumulation in lesions are also observed. These effects might also contribute to the diminishment of total lesions area as revealed by Oil Red O staining of this study.

Conclusion

The current study proposes a learning-based framework called DLDTI for identifying the association of drug targets. The structural characteristics of drug and the characteristics of the protein properties were firstly extracted. An automatic encoder-based model was then proposed for feature selection. Using this feature representation, a convolutional neural network architecture was proposed for predicting the DTI. The advantages of DLDTI were demonstrated by comparing it with three different methods. Experiments on DTI showed that the performance of DLDTI was better than that of the alternative method, which shows that the proposed learning-based framework was properly designed. Consistent with predicted results, the effects and molecular mechanism of TMPZ on atherosclerosis were experimentally confirmed in a novel animal model. With the source code and datasets available at https://github.com/CUMTzackGit/DLDTI, we hope this efficient and feasible computational methods to predict the potential associations between drugs and targets might be of great aid.

List of abbreviations

DTI: drug-target interaction; ROR-γt: retinoic-acid-receptor-related orphan receptor-gamma t; BLM: biparticle local model; TMPZ: tetramethylpyrazine; GIP: Gaussian interaction profile; GF: graph factorization; SAE: stack autoencoder; STRING: Search Tool for the Retrieval of Interacting Genes/Proteins; KEGG: Kyoto Encyclopedia of Genes and Genomes; GO: Gene Ontology; Ldlr: low-density lipoprotein receptor; HCHF: high-cholesterol and high-fat; PCR: polymerase chain reaction; WT: wild type; IHC: immunohistochemistry; SMC: smooth muscle cell; PRP: platelet-rich plasma

Declarations

Authors' contributions

ZYH conceived the project, conducted the experiment, and wrote the manuscript. KZ conceived the algorithm, conducted the experiment and wrote the manuscript. BYG,

LS, MMG, JG and YHW conducted the experiment. HQ analyzed the results. DZS and YZ supervised the study and revised the manuscript. All authors reviewed and approved the manuscript.

Competing interests

The authors declare that none of them have any competing interests.

Availability of data and materials

The source code and datasets available at https://github.com/CUMTzackGit/DLDTI.

Ethics approval and consent to participate

Not applicable.

Consent for publication

Not applicable.

Fundings

This work was funded by the National Natural Science Foundation of China, grant (No. 81703927) and the Fundamental Research Funds for the Central public welfare research institutes of China, grant (No. ZZ13-YQ-008).

Acknowledgements

Dr. Jerry, a professional English editor, provided language help and writing assistance.

References:

[1] Avorn J. The $2.6 Billion Pill — Methodologic and Policy Considerations. N Engl J Med 2015;372:1877–9.

[2] Munos B. Lessons from 60 years of pharmaceutical innovation. Nat Rev Drug Discov 2009;8:959–68..

[3] Nowak-Sliwinska P, Scapozza L, Ruiz i Altaba A. Drug repurposing in oncology:

561 Compounds, pathways, phenotypes and computational approaches for colorectal
562 cancer. Biochim Biophys Acta - Rev Cancer 2019;1871:434–54.

563 [4] Sleire L, Førde HE, Netland IA, Leiss L, Skeie BS, Enger PØ. Drug repurposing
564 in cancer. Pharmacol Res 2017;124:74–91.

565 [5] Ianculescu I, Weisman MH. The role of methotrexate in psoriatic arthritis: What
566 is the evidence? Clin Exp Rheumatol 2015;33:94–7.

567 [6] Corbett A, Smith J, Ballard C. New and emerging treatments for Alzheimers
568 disease. Expert Rev Neurother 2012;12:535–43.

569 [7] Santos R, Ursu O, Gaulton A, Bento AP, Donadi RS, Bologa CG, et al. A
570 comprehensive map of molecular drug targets. Nat Rev Drug Discov 2017;16:19–34.

571 [8] Duran C, Daminelli S, Thomas J, Joachim Haupt V, Schroeder M, Cannistraci CV.
572 Pioneering topological methods for network-based drug-target prediction by
573 exploiting a brain-network self-organization theory. Brief Bioinform 2017;19:1183–
574 202.

575 [9] Luo Y, Zhao X, Zhou J, Yang J, Zhang Y, Kuang W, et al. A network integration
576 approach for drug-target interaction prediction and computational drug repositioning
577 from heterogeneous information. Nat Commun 2017;8:573.

578 [10]Zeng X, Zhu S, Lu W, Liu Z, Huang J, Zhou Y, et al. Target identification among
579 known drugs by deep learning from heterogeneous networks. Chem Sci
580 2020;11:1775–97.

581 [11]Bleakley K, Yamanishi Y. Supervised prediction of drug-target interactions using
582 bipartite local models. Bioinformatics 2009;25:2397–403..

583 [12]Mei JP, Kwoh CK, Yang P, Li XL, Zheng J. Drug-target interaction prediction by
584 learning from local information and neighbors. Bioinformatics 2013;29:238–45.

585 [13]Gönen M. Predicting drug-target interactions from chemical and genomic kernels

using Bayesian matrix factorization. Bioinformatics 2012;28:2304–10.

[14] Wan F, Hong L, Xiao A, Jiang T, Zeng J. NeoDTI: Neural integration of neighbor information from a heterogeneous network for discovering new drug-target interactions. Bioinformatics 2019;35:104–11.

[15] Guo M, Liu Y, Shi D. Cardiovascular Actions and Therapeutic Potential of Tetramethylpyrazine (Active Component Isolated from Rhizoma Chuanxiong): Roles and Mechanisms. Biomed Res Int 2016;2016.

[16] Duan J, Xiang D, Luo H, Wang G, Ye Y, Yu C, et al. Tetramethylpyrazine suppresses lipid accumulation in macrophages via upregulation of the ATP-binding cassette transporters and downregulation of scavenger receptors. Oncol Rep 2017;38:2267–76.

[17] Zhang Y, Ren P, Kang Q, Liu W, Li S, Li P, et al. Effect of tetramethylpyrazine on atherosclerosis and SCAP/SREBP-1c signaling pathway in ApoE-/- mice fed with a high-fat diet. Evidence-Based Complement Altern Med 2017;2017.

[18] Jiang F, Qian J, Chen S, Zhang W, Liu C. Ligustrazine improves atherosclerosis in rat via attenuation of oxidative stress. Pharm Biol 2011;49:856–63.

[19] Libby P, Buring JE, Badimon L, Hansson GK, Deanfield J, Bittencourt MS, et al. Atherosclerosis. Nat Rev Dis Prim 2019;5:1–18.

[20] Wishart DS, Feunang YD, Guo AC, Lo EJ, Marcu A, Grant JR, et al. DrugBank 5.0: A major update to the DrugBank database for 2018. Nucleic Acids Res 2018;46:D1074–82.

[21] Zheng K, Wang L, You ZH. CGMDA: An Approach to Predict and Validate MicroRNA-Disease Associations by Utilizing Chaos Game Representation and LightGBM. IEEE Access 2019;7:133314–23.

[22] Zheng K, You Z-H, Wang L, Li Y-R, Wang Y-B, Jiang H-J. MISSIM: Improved miRNA-Disease Association Prediction Model Based on Chaos Game Representation

612 and Broad Learning System. In: Intelligent Computing Methodologies:2019

613 [23] Szklarczyk D, Gable AL, Lyon D, Junge A, Wyder S, Huerta-Cepas J, et al.
614 STRING v11: Protein-protein association networks with increased coverage,
615 supporting functional discovery in genome-wide experimental datasets. Nucleic Acids
616 Res 2019;47:D607–13.

617 [24] Zheng K, You Z-H, Li J-Q, Wang L, Guo Z-H, Huang Y-A. iCDA-CGR:
618 Identification of circRNA-disease associations based on Chaos Game Representation.
619 PLOS Comput Biol 2020;16:e1007872.

620 [25] Zheng K, You Z, Wang L, Wong L, Chen Z. Inferring Disease-Associated
621 Piwi-Interacting RNAs via Graph Attention Networks. bioRxiv 2020.01.08.898155;
622 https://doi.org/10.1101/2020.01.08.898155

623 [26] Ahmed A, Shervashidze N, Narayanamurthy S, Josifovski V, Smola AJ.
624 Distributed large-scale natural graph factorization. In: Proceedings of the 22nd
625 International World Web Conference (WWW 2013):2013

626 [27] Shin HC, Orton MR, Collins DJ, Doran SJ, Leach MO. Stacked autoencoders for
627 unsupervised feature learning and multiple organ detection in a pilot study using 4D
628 patient data. IEEE Trans Pattern Anal Mach Intell 2013;35:1930–43.

629 [28] Zheng K, You Z-H, Wang L, Zhou Y, Li L-P, Li Z-W. MLMDA: a machine
630 learning approach to predict and validate MicroRNA–disease associations by
631 integrating of heterogenous information sources. J Transl Med 2019;17:260.

632 [29] Yann L, Yoshua B. Convolutional Networks for Images, Speech, and Time-Series
633 In: The Handbook of Brain Theory and Neural Networks:1995

634 [30] Stelzer G, Rosen N, Plaschkes I, Zimmerman S, Twik M, Fishilevich S, et al. The
635 GeneCards suite: From gene data mining to disease genome sequence analyses. Curr
636 Protoc Bioinforma 2016;2016:1.30.1-1.30.33.

637 [31] Guo X, Gao M, Wang Y, Lin X, Yang L, Cong N, et al. LDL Receptor

638 Gene-ablated Hamsters: A Rodent Model of Familial Hypercholesterolemia With
639 Dominant Inheritance and Diet-induced Coronary Atherosclerosis. EBioMedicine
640 2018;27:214–24.

641 [32]Liu X, Li J, Liao J, Wang H, Huang X, Dong Z, et al. Gpihbp1 deficiency
642 accelerates atherosclerosis and plaque instability in diabetic Ldlr -/- mice.
643 Atherosclerosis 2019;282:100–9.

644 [33]Kuzuya M, Nakamura K, Sasaki T, Xian WC, Itohara S, Iguchi A. Effect of
645 MMP-2 deficiency on atherosclerotic lesion formation in apoE-deficient mice.
646 Arterioscler Thromb Vasc Biol 2006;26:1120–5.

647 [34]Pleines I, Elvers M, Strehl A, Pozgajova M, Varga-Szabo D, May F, et al. Rac1 is
648 essential for phospholipase C-γ2 activation in platelets. Pflugers Arch Eur J Physiol
649 2009;457:1173–85.

650 [35]Guo G, Wang H, Bell D, Bi Y, Greer K. KNN model-based approach in
651 classification. In: On The Move to Meaningful Internet Systems 2003:2003

652 [36]Svetnik V, Liaw A, Tong C, Christopher Culberson J, Sheridan RP, Feuston BP.
653 Random Forest: A Classification and Regression Tool for Compound Classification
654 and QSAR Modeling. J Chem Inf Comput Sci 2003;43:1947–58.

655 [37]Freund Y, Schapire RE. A Decision-Theoretic Generalization of On-Line
656 Learning and an Application to Boosting. J Comput Syst Sci 1997;55:119–39.

657 [38]Offermanns S. Activation of platelet function through G protein-coupled
658 receptors. Circ Res 2006;99:1293–304.

659 [39]Ballerini P, Dovizio M, Bruno A, Tacconelli S, Patrignani P. P2Y12 receptors in
660 tumorigenesis and metastasis. Front Pharmacol 2018;9:1–8.

661 [40]Geovanini GR, Libby P. Atherosclerosis and inflammation: Overview and updates.
662 Clin Sci 2018;132:1243–52.

[41]Otsuka F, Yasuda S, Noguchi T, Ishibashi-Ueda H. Pathology of coronary atherosclerosis and thrombosis. Cardiovasc Diagn Ther 2016;6:396–408.

[42]Xiang B, Zhang G, Liu J, Morris AJ, Smyth SS, Gartner TK, et al. A Gi-independent mechanism mediating Akt phosphorylation in platelets. J Thromb Haemost 2010;8:2032–41.

[43]Zhao Y, Qu H, Wang Y, Xiao W, Zhang Y, Shi D. Small rodent models of atherosclerosis. Biomed Pharmacother 2020;129:110426.

[44]Fuentes EQ, Fuentes FQ, Andrés V, Pello OM, De Mora JF, Palomo IG. Role of platelets as mediators that link inflammation and thrombosis in atherosclerosis. Platelets 2013;24:255–62.

[45]Freynhofer MK, Iliev L, Bruno V, Rohla M, Egger F, Weiss TW, et al. Platelet turnover predicts outcome after coronary intervention. Thromb Haemost 2017;117:923–33.

Additional files:

File name: table 1

File format: .xlsx

Tile of data: Complete results of GO and KEGG analysis

Description of data: Results of KEGG analysis are included in sheet 1, and those of GO analysis are included in sheet 2.

File name: table 2

File format: .xlsx

Tile of data: Complete results of predicted targets of TMPZ

Description of data: 288 predicted targets of TMPZ on atherosclerosis are included in sheet 1, and 190 proteins among the afore-mentioned targets are also involved in the

platelet activation process, which are included in sheet 2.

Figures

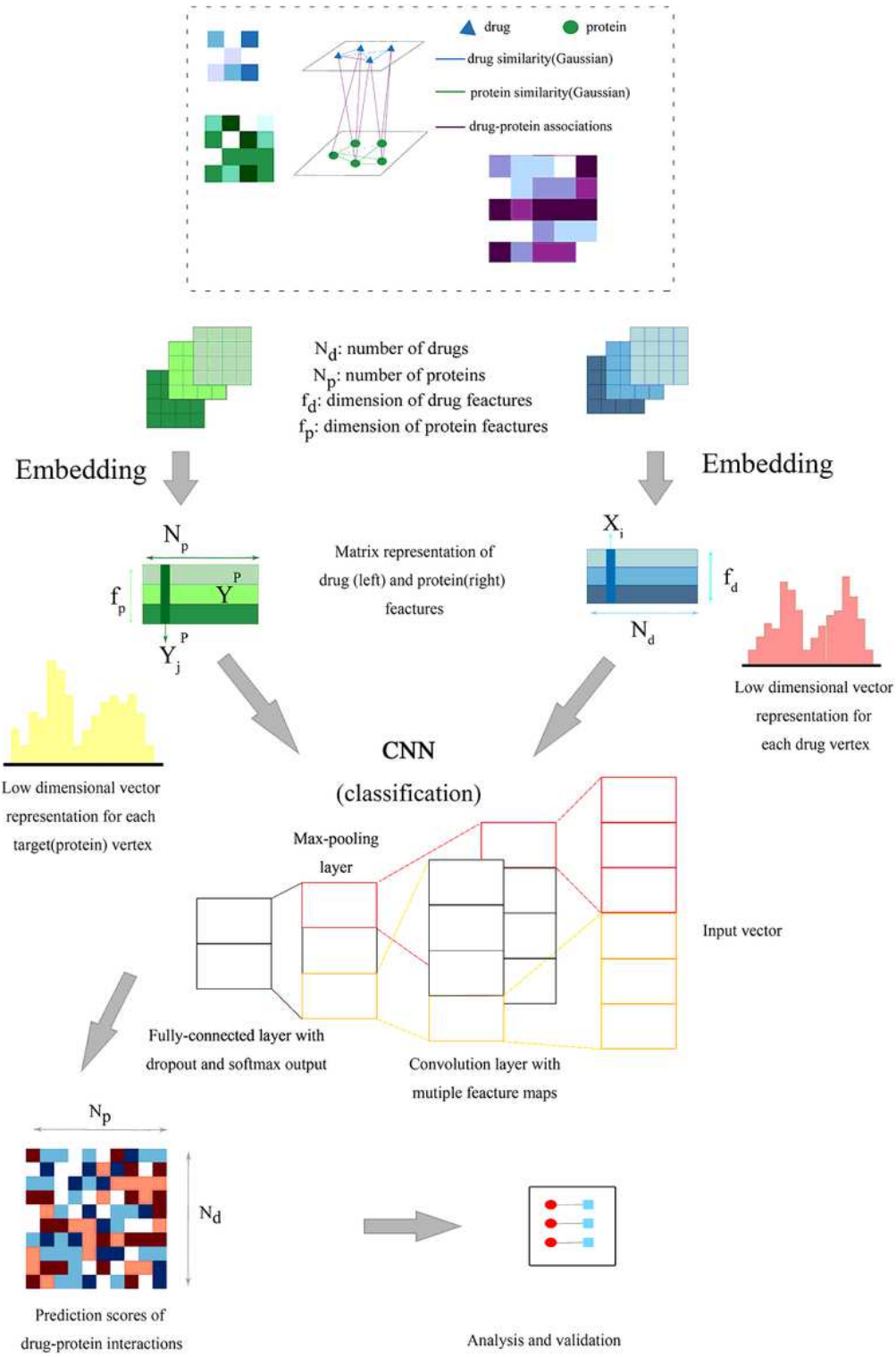

Figure 1

The flowchart of the DLDTI pipeline. DLDTI first integrates a variety of drug-related information sources to construct a heterogeneous network and applies a compact feature learning algorithm to obtain a low-dimensional vector representation of the features describing the topological properties for each node.

Next, DLDTI determines the optimal mapping from the plenary mapping space to the prediction subspace, and whether the feature vector is close to the known correlations. Afterwards, DLDTI infers the new DTIs by ranking the candidates according to their proximity to the predicted subspace.

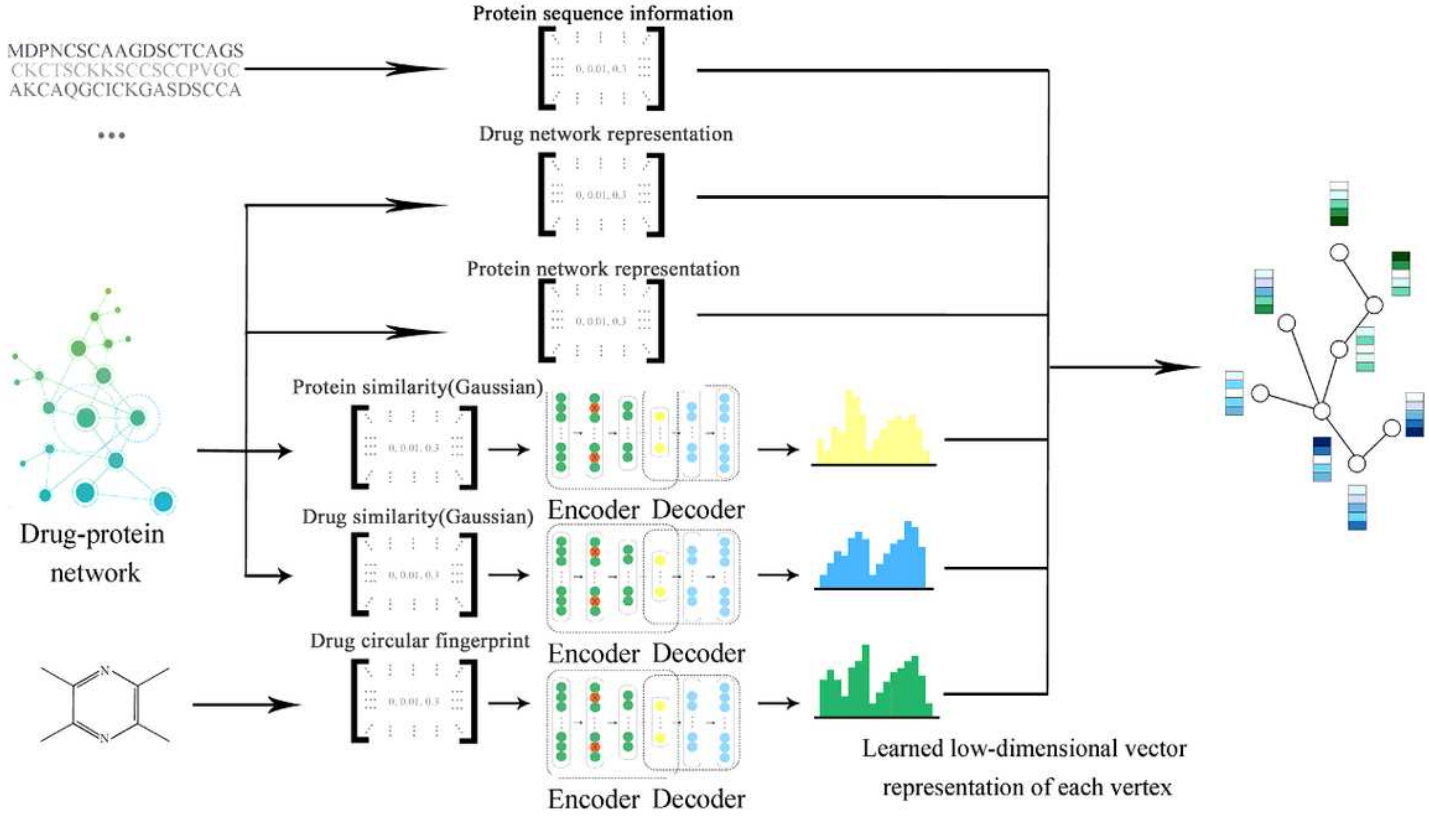

Figure 2

Schematic illustration of compact feature learning. The Node2Vec algorithm is firstly used to calculate the topology information in complex networks. GIP kernel similarity and drug structure information are then extracted by a stacked automatic encoder, and the heterogeneous information is integrated to obtain a low-dimensional representation of the feature vector of each node. The resulting low-dimensional descriptor integrates the attribute characteristics, interaction information, relationship attributes and network topology of each protein or target node in the complex network.

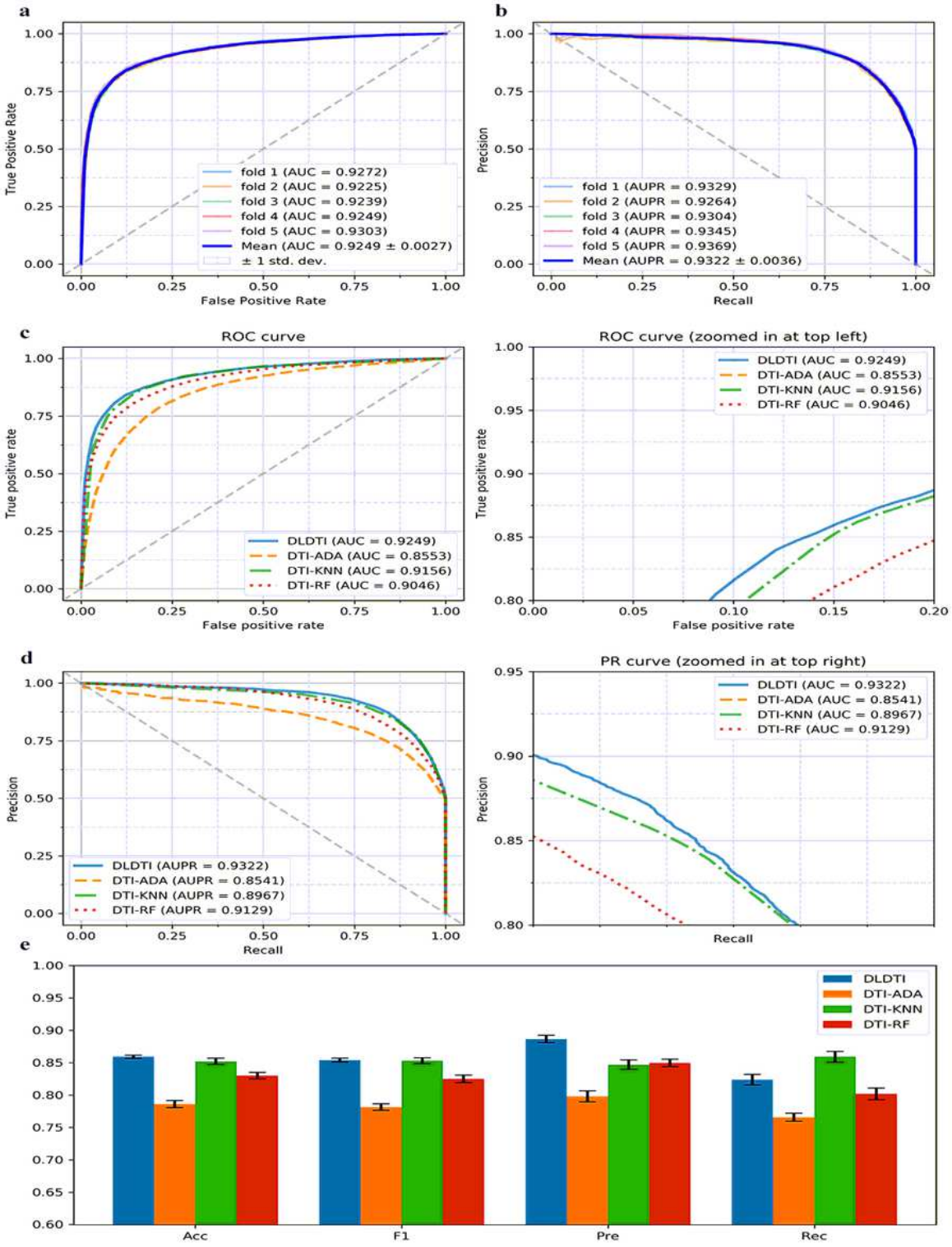

Figure 3

Performance of DLDTI. (a) ROC curves performed by DLDTI model on DrugBank dataset. (b) PR curves performed by DLDTI model on DrugBank dataset. (c) Performance comparison (AUC scores) among four different prediction model which are DTI-ADA, DTI-KNN, and DTI-RF.(d)Performance comparison (AUPR scores) among four different prediction models including DTI-ADA, DTI-KNN, and DTI-RF.(e)Performance comparison (Acc., F1, Pre., Rec. scores) among DTI-ADA, DTI-KNN, and DTI-RF prediction models.

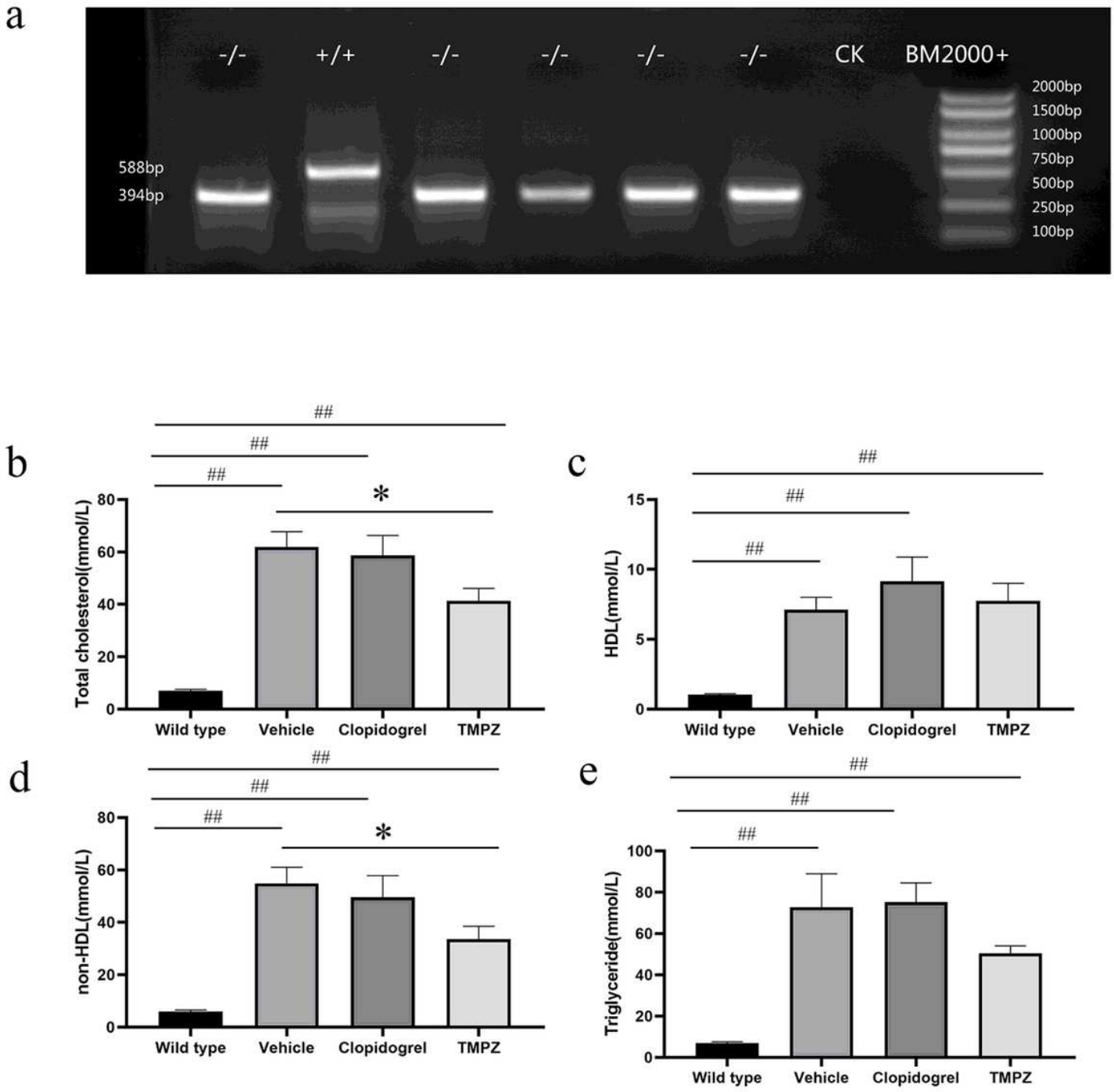

Figure 4

Genotyping and lipid parameters between different groups. (a) PCR analysis was performed using ear genomic DNA from WT (+/+) and homozygote (−/−) with the Δ194 deletion. The concentrations of plasma TC (b), HDL(c), non-HDL(d) and TG(e) were measured in WT, vehicle, TMPZ and clodipogrel groups at the endpoint of this experiment. Differences were assessed by unpaired student t's test or Mann-Whitney test. * p<0.05 versus Vehicle, **p<0.01 versus Vehicle. ##p<0.01 versus WT.

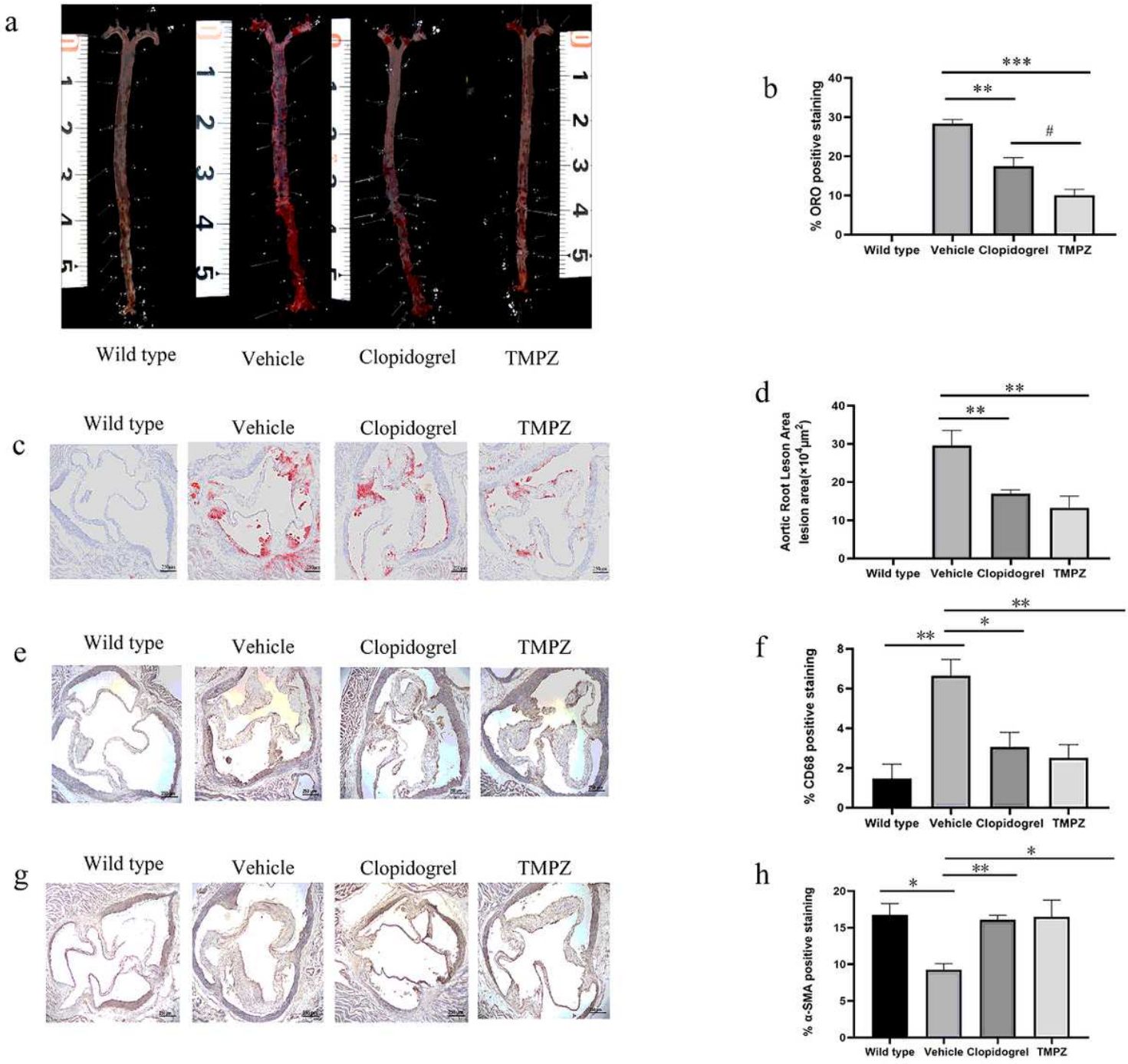

Figure 5

Histological analysis. (a) Representative images of en face analysis. n=6. (b) Quantitative analysis of lesion areas in whole aortas. Differences were assessed by unpaired student t's test. (c) Representative images of Oil Red O staining of aortic root sections. (d) Quantitative analysis of lesion areas in aortic root sections. (e) Representative images of macrophage (CD68) analysis (b) Quantitative analysis of lesions area in macrophage analysis. (f) Representative images of SMC (SMA) analysis (g) Quantitative analysis of lesions area in SMC. Differences were assessed by unpaired student t's test. * p<0.05 versus Vehicle, **p<0.01 versus Vehicle. #p<0.05 versus clopidogrel. Scale bar=250μm. n=3.

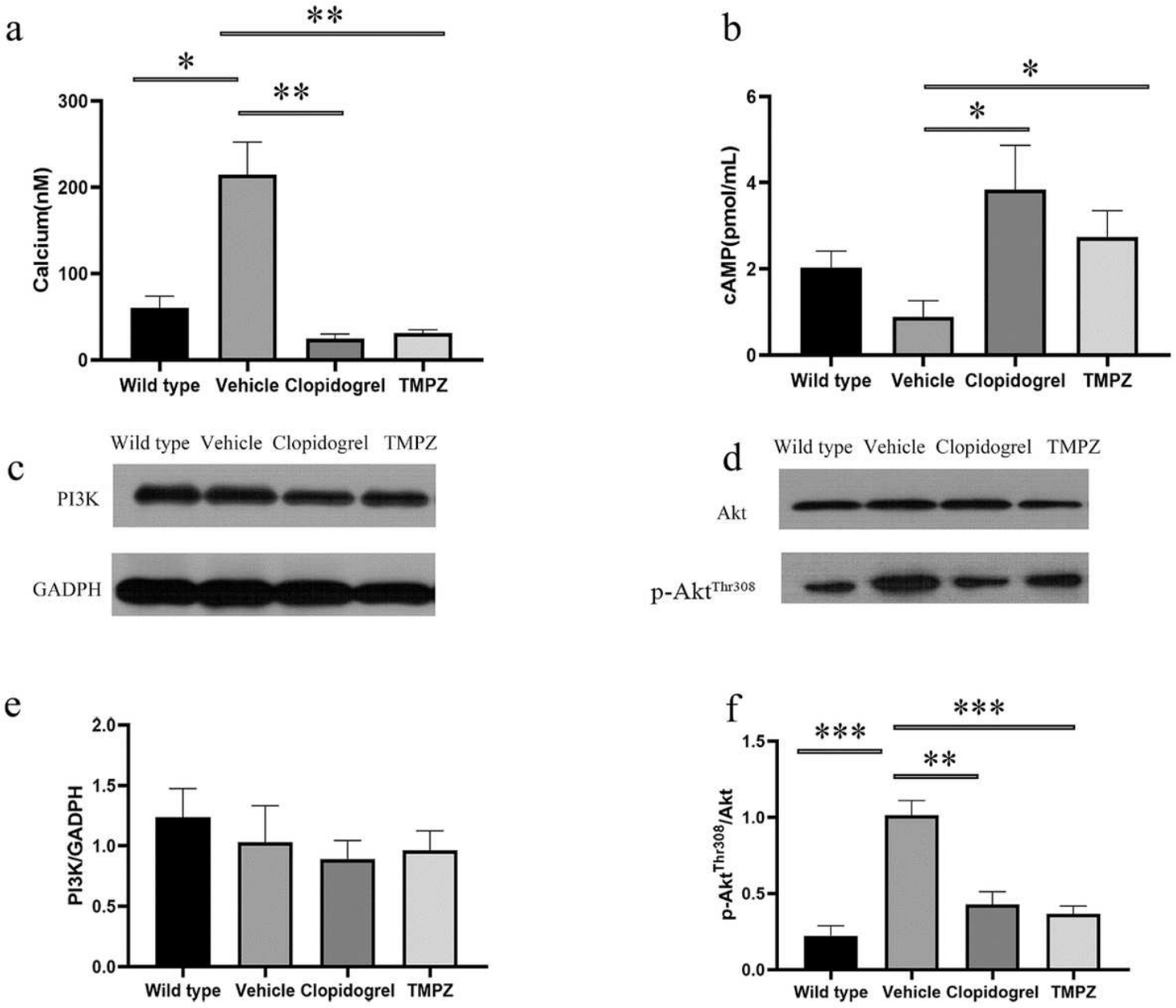

Figure 6

Signaling transduction in ADP-mediated platelet activation. (a) Intracellular calcium concentration. (b) Intracellular cAMP concentration. Western blot analyses of the expression of PI3K (c), Akt (d) and p-Akt (d). Differences were assessed by unpaired student t's test with or without Welch's corrections. ** $p<0.01$ versus Vehicle, * $p<0.05$ versus Vehicle. n=4-6.

Supplementary Files

This is a list of supplementary files associated with this preprint. Click to download.

- SItable2.xlsx
- SItable1.xlsx